



Papers published in *Ocean Science Discussions* are under  
open-access review for the journal *Ocean Science*

**OSD**

3, 609–636, 2006

---

**SSH Variability in the  
North Atlantic**

D. Cromwell

---

# Temporal and spatial characteristics of sea surface height variability in the North Atlantic Ocean

**D. Cromwell**

Ocean Observing and Climate National Oceanography Centre, Southampton (NOCS), Room 254/35, European Way, Southampton, SO14 3ZH, UK

Received: 29 March 2006 – Accepted: 8 May 2006 – Published: 21 June 2006

Correspondence to: D. Cromwell (ddc@noc.soton.ac.uk)

[Title Page](#)

[Abstract](#)

[Introduction](#)

[Conclusions](#)

[References](#)

[Tables](#)

[Figures](#)

◀

▶

◀

▶

[Back](#)

[Close](#)

[Full Screen / Esc](#)

[Printer-friendly Version](#)

[Interactive Discussion](#)

EGU

## Abstract

We investigate the spatial and temporal variability of sea surface height (SSH) in the North Atlantic basin using altimeter data from October 1992–January 2004. Our primary aim is to provide a fuller description of such variability, particularly that associated with propagating signals. We also investigate possible correlations between SSH variability and climate indices.

We first investigate interannual SSH variations by deriving the complex empirical orthogonal functions (CEOFs) of altimeter data lowpass-filtered at 18 months. We determine the spatial structure of the leading four modes (both in amplitude and phase) and also the associated principal components (PCs). Using wavelet analysis we derive the time-varying spectral density of the PCs revealing when particular modes are strongest between 1992–2004. The spatial pattern of the leading CEOF, comprising 30% of the total variability, has a 5-year period. Signal propagation with a 5-year period is also observed in the Labrador Sea. The second mode, with a dominant 3-year signal, has strong variability in the eastern basin.

We next focus on the Azores subtropical frontal region. The leading mode (35%) is strong in the south and east of this region. The second mode (21%) has a near-zonal band of low variance between  $\sim 22^{\circ}$ – $27^{\circ}$  N sandwiched between two regions of high variance. We then lowpass filter the altimeter data at a cutoff of 30 days, instead of 18 months, in order to retain signals associated with propagating baroclinic Rossby waves. The leading mode is the annual steric signal, around 46% of the SSH variability. The third and fourth CEOFs,  $\sim 11\%$  of the remaining variability, are associated with westward propagation which is particularly dominant in a “waveband” between  $32^{\circ}$ – $36^{\circ}$  N.

No significant cross-correlation is found between the North Atlantic Oscillation index and the amplitude of the leading two principal components of interannual SSH variability. The East Atlantic Pattern index, however, is correlated with the principal components of the two leading modes of SSH variability, particularly with PC2 in the Azores

OSD

3, 609–636, 2006

---

## SSH Variability in the North Atlantic

D. Cromwell

---

[Title Page](#)

[Abstract](#)

[Introduction](#)

[Conclusions](#)

[References](#)

[Tables](#)

[Figures](#)

◀

▶

◀

▶

[Back](#)

[Close](#)

[Full Screen / Esc](#)

[Printer-friendly Version](#)

[Interactive Discussion](#)

EGU

subtropical frontal region. Further investigation of forcing mechanisms is suggested using hindcasts from ocean general circulation models.

OSD

3, 609–636, 2006

## 1 Introduction

The ocean circulation and dynamics of the North Atlantic Ocean play an important role in the climate system. In particular, the significance of the thermohaline circulation “global conveyor belt”, which carries warm water north towards the poles and returns cold water at depth, is well known (Broecker, 1991). Much recent interest has focused on the meridional overturning circulation (Schiermeier, 2006) and, in particular, on the finding that the MOC at 25° N has apparently slowed by around 30% (Bryden, 2005).

Levermann et al. (2005) suggest on the basis of modelling studies that a weakening of the thermohaline circulation could generate dynamic sea surface height (SSH) changes that locally reach up to ~1 m. According to Häkkinen and Rhines (2004), in the last two decades there has been an increase in SSH in the North Atlantic subpolar gyre, and a reduction in the strength of the North Atlantic subpolar gyre in the 1990s. However, they stressed that because of the lack of SSH data prior to 1978, there is uncertainty as to whether or not this feature is a decadal cycle or a long-term trend.

Although this study does not tackle these issues directly, our aim is to provide an improved quantitative description of spatial and temporal SSH variability in the North Atlantic, a necessary step towards being able to detect unambiguously any long-term trends. In particular, we aim to provide an improved description of SSH variability associated with propagating signals: an important means by which one part of the ocean-atmosphere system communicates with another (Gill, 1982; Jacobs et al., 1994).

The paper is structured as follows. In Sect. 2.1 we describe the data. We apply two well-established methods in geophysical signal processing: complex empirical orthogonal function decomposition and wavelet analysis. CEOF analysis (Sect. 2.2) yields information on the observed spatial and temporal variability in SSH, particularly where propagating features, such as baroclinic Rossby waves, are known to contribute to

## SSH Variability in the North Atlantic

D. Cromwell

[Title Page](#)

[Abstract](#)

[Introduction](#)

[Conclusions](#)

[References](#)

[Tables](#)

[Figures](#)

[◀](#)

[▶](#)

[◀](#)

[▶](#)

[Back](#)

[Close](#)

[Full Screen / Esc](#)

[Printer-friendly Version](#)

[Interactive Discussion](#)

EGU

variability. Wavelet analysis (Sect. 2.3) reveals the time-varying spectral content of SSH signatures. We present our results in Sect. 3. In Sect. 3.1 we investigate the interannual SSH variability in the North Atlantic Ocean. In Sect. 3.2, we focus on the dynamic region around the Azores subtropical front. Here we investigate both inter-  
5 annual variability as well as subannual variability associated with Rossby waves. In Sect. 3.3, we investigate possible links between the observed SSH variability and two leading modes of atmospheric variability, represented by the North Atlantic Oscillation and East Atlantic Pattern climate indices. Finally, we summarise and discuss the results in Sect. 4.

## 10 2 Data and methodology

### 2.1 Data description

We use the merged altimeter data product known as DUACS (Developing Use Of Altimetry For Climate Studies) which incorporates altimeter data from the ERS and TOPEX/Poseidon satellites and their successors, respectively Envisat and Jason. The  
15 DUACS dataset was produced by the CLS Space Oceanography Division and AVISO, the French space agency. The data are sea surface height anomalies and are provided on a Mercator spatial grid of  $(1/3)^\circ$  longitude  $\times (1/3)^\circ \cos(\text{latitude})$ . The temporal sampling of the data is 7 days, and the period covered is October 1992–January 2004.  
20 Details of the data processing and mapping method can be found in Le Traon and Ogor (1998) and Le Traon et al. (1998). The reader is also referred to the DUACS handbook, [http://www.jason.oceanobs.com/documents/donnees/duacs/handbook\\_duacs\\_uk.pdf](http://www.jason.oceanobs.com/documents/donnees/duacs/handbook_duacs_uk.pdf), and to CLS (2004) for further details.

### 25 2.2 Complex empirical orthogonal function analysis

Empirical orthogonal function (EOF) analysis allows one to decompose a dataset in terms of its statistical modes of variability. These modes are obtained by performing

[Title Page](#)

[Abstract](#)

[Introduction](#)

[Conclusions](#)

[References](#)

[Tables](#)

[Figures](#)

[◀](#)

[▶](#)

[◀](#)

[▶](#)

[Back](#)

[Close](#)

[Full Screen / Esc](#)

[Printer-friendly Version](#)

[Interactive Discussion](#)

an eigenvalue analysis of the covariance matrix of the data. This yields eigenvectors, which can be mapped as spatial patterns of variability, and associated principal components (PCs), each of which describe the time-evolution of the corresponding spatial structure.

5 In complex EOF analysis we first “complexify” the data. Thus, if  $X_t$  is the original real time series that we are interested in (SSH variations, for example), then we generate a related time series:  $X_t \Rightarrow X_t + iX_t^H$  where  $X_t^H$  is the Hilbert transform of the original data (von Storch and Zwiers, 1999). We can then apply conventional eigentechniques, such as EOFs, to the complexified time series. This yields statistical patterns that contain  
10 both real and imaginary components. It is more physically meaningful to represent the data decomposition in terms of amplitude and phase. This treatment also naturally lends itself to examination of any propagating phenomena in the original data. Determining propagation in SSH variations is an important focus of the present study. Moreover, as Fu (2004) notes, the complex EOF approach is more efficient than a regular EOF analysis because of the importance of capturing the phase information in the  
15 SSH variability.

The convention adopted in this study is that progression in time corresponds to anti-clockwise rotation of the eigenvector phase. Note that, because zero phase angle is an arbitrary choice, the direction of a phase arrow at any particular geographical  
20 location is unimportant. What matters is whether, and in what sense, the direction of the phase arrow changes between one location and another. Thus, if a spatial region of strong SSH signal has the phase arrows rotating anti-clockwise from east to west, this indicates a strong westward propagating signal. Tourre et al. (1998) used complex EOFs in their study of interdecadal variation and propagating features in the  
25 Pacific Ocean (but note that they used the opposite sign convention for rotation of phase arrows and direction of propagation).

To summarise: complex EOF analysis yields, for each statistical mode, a map of the complex-valued spatial variability pattern (i.e. both amplitude and phase) as well as an associated complex principal component (PC) which can be plotted as a time series of

---

SSH Variability in the  
North Atlantic

D. Cromwell

---

[Title Page](#)

[Abstract](#)

[Introduction](#)

[Conclusions](#)

[References](#)

[Tables](#)

[Figures](#)

◀

▶

◀

▶

[Back](#)

[Close](#)

[Full Screen / Esc](#)

[Printer-friendly Version](#)

[Interactive Discussion](#)

amplitude and phase values. Anticlockwise rotation of the phase arrow between one spatial location and another indicates progression in time. As we see in the following section, a wavelet analysis of the PC can be performed thereafter to yield the time-varying spectral content of the associated complex EOF mode.

### 5 2.3 Wavelet analysis

The wavelet method allows one to analyse localised power variations within a discrete series at a range of scales (Foufoula-Georgiou and Kumar, 1994). Wavelets can be considered as building blocks in a decomposition or series expansion using dilated and translated versions of a mother wavelet, each multiplied by an appropriate coefficient (Farge, 1992). The local wavelet power spectrum is the square of the wavelet coefficients (Torrence and Compo, 1998). The global wavelet spectrum is the average spectrum over all time, equivalent to the Fourier spectrum. We make the usual choice here of adopting the Morlet wavelet, a complex-valued, modulated Gaussian plane wave widely used in the study of geophysical processes. It is described by  $15 \psi(\eta) = \pi^{-1/4} e^{i\omega\eta} e^{-\eta^2/2}$ , where  $\omega$  is the nondimensional frequency which must be equal to, or greater than, 5 to satisfy the wavelet admissibility condition (Farge, 1992).

## 3 Results of data analysis

### 3.1 Interannual sea surface height variability in the North Atlantic Ocean

We focus first on the interannual sea surface height variability in the North Atlantic   
20 Ocean region spanning  $10^\circ$ – $65^\circ$  N,  $80^\circ$ – $0^\circ$  W. The data are lowpass filtered to remove variability with periods shorter than 18 months. The data is then regridded to  $1^\circ \times 1^\circ$  (retaining the original high-resolution DUACS gridding exceeded our computing capacity to perform CEOF analysis for the whole North Atlantic basin). Our initial approach has similarities to that of Fu (2004) who studied the interannual SSH variation in the

OSD

3, 609–636, 2006

## SSH Variability in the North Atlantic

D. Cromwell

[Title Page](#)

[Abstract](#)

[Introduction](#)

[Conclusions](#)

[References](#)

[Tables](#)

[Figures](#)

◀

▶

◀

▶

[Back](#)

[Close](#)

[Full Screen / Esc](#)

[Printer-friendly Version](#)

[Interactive Discussion](#)

EGU

North Atlantic; however there are significant differences. For example, we extend the analysis of SSH variability in that we investigate not just the leading CEOF mode but the first four modes for a more complete description. This is further enhanced by applying wavelet analysis to determine the time-varying spectral content of the principal components. Moreover, in the next section, we home in on the dynamic Azores subtropical frontal region of the northeast Atlantic. Note that in this particular region we apply filtering that retains the baroclinic Rossby wave signal, unlike Fu (2004).

First, consider the results of the CEOF analysis for the whole North Atlantic basin. In Fig. 1 we plot the spatial patterns of the leading four CEOFs. Recall that the modes are complex-valued; we plot both the spatial CEOF amplitude (coloured contours) and phase (arrows). In Fig. 2, we plot the complex-valued time series of the associated principal components: amplitude (green line) and phase (blue circles) time series are plotted for each. The leading CEOF mode represents 30% of the total SSH variability, and the sum of the first four modes accounts for 74%. We use the Lambert conical projection for the maps as it takes account of the latitudinal variation in length of a fixed range of degrees in longitude.

It can be seen from Fig. 2 that the phase time series of PC1 (the principal component of the leading CEOF mode) has a dominant period of around 5 years. Looking at the corresponding amplitude map in Fig. 1, we note that there is a tripole-like structure: two domains of high SSH variability in the subpolar gyre and at low latitudes, with a region of low variability between them. The two high variability regions at high and low latitudes are linked by a ridge of high variability along the eastern boundary. It is well known that there is a sea surface temperature tripole associated with the North Atlantic Oscillation (Marshall et al., 2001). However, although there appears to be a degree of similarity between the patterns in SST and the leading-mode SSH, the structures are not the same.

There is some indication that the phase arrows in the leading-mode SSH along the eastern boundary rotate anticlockwise (a shift from pointing predominantly north off the African coast to northwest off the British Isles). This suggests that there is propa-

## SSH Variability in the North Atlantic

D. Cromwell

[Title Page](#)

[Abstract](#)

[Introduction](#)

[Conclusions](#)

[References](#)

[Tables](#)

[Figures](#)

◀

▶

◀

▶

[Back](#)

[Close](#)

[Full Screen / Esc](#)

[Printer-friendly Version](#)

[Interactive Discussion](#)

EGU

gating energy running northwards along the eastward boundary linking the subtropics and subpolar regions. There is also evidence of SSH propagation in the northwest Atlantic and Labrador Sea: a clear anticlockwise rotation of phase arrows as the location changes north from Newfoundland towards the west of Greenland.

5 The spatial pattern of the second CEOF (17% of the total variability) has a different structure from the leading CEOF. The regions of high variability are concentrated in the eastern subtropical gyre between  $\sim 30^\circ$ – $40^\circ$  N and in the tropics ( $\sim 5^\circ$ – $15^\circ$  N). The structure of SSH variability, with highs in the eastern basin, suggests a possible link with the East Atlantic Pattern. This is the second most prominent mode (after the NAO)  
10 of low-frequency atmospheric pressure variability over the North Atlantic (Barnston and Livezey, 1987). We look at possible connections with climate indices in further detail in Sect. 3.3. As we see from Fig. 2, the phase time series of PC2 has a cycle of  $\sim 3$  years. We analyse the time-varying spectral energy of this time series by subjecting it to a wavelet analysis, the results of which are shown in Fig. 3 (in fact, the leading  
15 four PCs were subject to wavelet analysis to provide summary descriptions for Table 1, but we only show the results for PC2 here). From top to bottom, we see: (a) the input time series (i.e. the phase of PC2); (b) the wavelet power spectrum of (a), where the dashed line indicates the cone of influence below which edge effects, arising from the finite length of the time series, become important (Torrence and Compo, 1998); (c) the  
20 global wavelet power spectrum, i.e. time integral of (b); (d) time series of the scale average of (b) in the period range 2.5–3.5 years (to capture the dominant cycle of  $\sim 3$  years). In Table 1, we summarise the characteristics of all four leading modes for the 18-month lowpass filtered data in the North Atlantic Ocean.

### 3.2 Sea surface height variability in the Azores subtropical front

#### 25 3.2.1 Interannual variability: lowpass filtering at 18 months

We now focus on the northeast Atlantic ( $20^\circ$ – $40^\circ$  N,  $50^\circ$ – $10^\circ$ W), encompassing the Azores subtropical front. This region is rich in westward propagating Rossby waves

OSD

3, 609–636, 2006

---

## SSH Variability in the North Atlantic

D. Cromwell

---

[Title Page](#)

[Abstract](#)

[Introduction](#)

[Conclusions](#)

[References](#)

[Tables](#)

[Figures](#)

[◀](#)

[▶](#)

[◀](#)

[▶](#)

[Back](#)

[Close](#)

[Full Screen / Esc](#)

[Printer-friendly Version](#)

[Interactive Discussion](#)

EGU

and eddies (Tokmakian and Challenor, 1993; Cipollini et al., 1997; Pingree 1997; Cipollini et al., 1998; Tychensky et al., 1998; Pingree 2002). Given the smaller geographical domain, we now have sufficient computing capacity to calculate CEOFs for the DUACS dataset at its original high-resolution spatial gridding of  $(1/3)^\circ$  longitude  $\times (1/3)^\circ \times \cos(\text{latitude})$ . Figures 4 and 5, analogous to Figs. 1 and 2 respectively, show the results of the complex EOF analysis: amplitude and phase maps of the leading four CEOFs and the associated principal components. These four modes account for 79% of the total variability.

As shown in Fig. 4, the leading mode (35% of the total variability) is strong in the south and east, consistent with the NAO-related pattern found in Sect. 3.1 (North Atlantic basin). Variability strength is around one order of magnitude lower north of  $\sim 30^\circ$  N, except for the northeast region and a few isolated patches in the northwest quadrant. The second mode (21% of the total variability) has a different spatial distribution: a near-zonal band of lower variance between  $\sim 22^\circ$ – $27^\circ$  N sandwiched between two regions of higher variance. This reveals further details of the EAP-related structure found earlier. Again, the levels of variance span around one order of magnitude. Mode 3 has a strong ridge of variability near  $28^\circ$  N.

We performed wavelet analysis of the phase time series of all four leading principal components to investigate time-dependent spectral energy changes. Fig. 6 shows the results for the phase of the leading mode which displays strong propagation at  $\sim 3$  years and  $\sim 5$  years (though the latter must be treated with caution in this smaller geographical domain because it falls beneath the cone of influence). In Sect. 3.1 above we noted that the EAP-related mode (second leading mode) had a dominant timescale of  $\sim 3$  years. The discovery of a  $\sim 3$  year component in the leading mode of SSH variability in the subtropical Azores Frontal region suggests that the EAP may be playing a strong role here. The scale-averaged energy in the period range 2–4 years (to capture the  $\sim 3$  year signal) decays gradually from a peak in 1994. The characteristics of all four leading modes for the 18-month lowpass filtered data in the region of the Azores subtropical front are summarised in Table 2.

## SSH Variability in the North Atlantic

D. Cromwell

[Title Page](#)

[Abstract](#)

[Introduction](#)

[Conclusions](#)

[References](#)

[Tables](#)

[Figures](#)

◀

▶

◀

▶

[Back](#)

[Close](#)

[Full Screen / Esc](#)

[Printer-friendly Version](#)

[Interactive Discussion](#)

EGU

### 3.2.2 Subannual baroclinic propagation: lowpass filtering at 30 days

OSD

3, 609–636, 2006

As mentioned above, it is well known that westward propagating baroclinic Rossby waves can be seen in SSH observations in the mid-latitudes of the North Atlantic basin. In particular, a ‘waveband’ of enhanced SSH variability associated with such waves is concentrated in a quasi-zonal strip centred near 34° N (Cromwell, 2001). The period of these midlatitude waves are subannual (~6–10 months); lowpass filtering at 18 months would therefore remove them. To study these signals, we therefore lowpass filter the data with a cutoff of 30 days, rather than 18 months, thus retaining the baroclinic Rossby wave signal but removing higher-frequency variability. We then performed CEOF analysis followed by wavelet analysis of the principal components, just as before.

The leading mode is the annual steric signal which accounts for 46% of the total SSH variability. If this mode is discounted, the second mode has 10% of the remaining variability and has three significant timescales at ~3 years, ~1 years and 6 months (not plotted). The third mode (6% of non-steric variability) displays properties consistent with propagating baroclinic Rossby waves. Figure 7 shows the spatial pattern of this mode, including the westward direction of propagation. Note the concentration of SSH variability in a near zonal band at 32°–36° N. Note, too, the anticlockwise rotation of the phase vector from east to west, consistent with westward propagation in this region. We have thus found for the first time, as far as we are aware, the variation in the trajectory (in both longitude and latitude) of the propagation of Rossby waves in this region. By estimating the period (~230 days) of this mode from the associated principal component (not plotted here), and the spatial distance over which a 360° rotation of the phase arrow occurs, i.e. the wavelength (~520 km), we can estimate the speed of the Rossby waves at this latitude as ~2.7 cm/s. This confirms earlier estimates (Chelton and Schlax, 1996, Cipollini et al., 1997). CEOF mode 4 displays similar characteristics as mode 3, including the westward propagation. This indicates that the baroclinic Rossby wave energy is partitioned into both these modes, representing a total variabil-

## SSH Variability in the North Atlantic

D. Cromwell

[Title Page](#)

[Abstract](#)

[Introduction](#)

[Conclusions](#)

[References](#)

[Tables](#)

[Figures](#)

◀

▶

◀

▶

[Back](#)

[Close](#)

[Full Screen / Esc](#)

[Printer-friendly Version](#)

[Interactive Discussion](#)

EGU

ity of 11% of the non-steric SSH signal.

We then perform a wavelet analysis of the phase component of PC3, yielding detailed information about the phase propagation corresponding to the Rossby waves (Fig. 8). Figure 8b shows strong spectral content at the subannual periods characteristic of such waves at midlatitudes. There is also strong variability at periods of 2–4 years, though after 2001 this energy lies below the cone of influence (dashed line) and must be treated with caution (edge effects). In Fig. 8d, scale averaging over the period range of 0.5–0.8 years (~6–10 months) shows the time-varying strength of the Rossby wave signal. There are peaks in 1996, 1997, 1999 and again in 2003. These are likely related to peaks in forcing. Finally, the characteristics of all four leading modes for the 30-day lowpass filtered data in the region of the Azores subtropical front are summarised in Table 3.

### 3.3 Relationship of the North Atlantic Oscillation (NAO) and East Atlantic Pattern (EAP) to Sea Surface Height Variability

Atmospheric pressure variations play a role in forcing sea surface height variability. To investigate a possible physical relationship between modes of atmospheric variability and SSH variability we used the climate indices provided by the National Oceanic and Atmospheric Administration/National Weather Service Climate Prediction Center (CPC). The two leading atmospheric pressure modes in winter are the North Atlantic Oscillation (NAO) and East Atlantic Pattern (EAP). The CPC indices are available from <http://www.cpc.ncep.noaa.gov/> and are derived from an analysis based on the work of (Barnston and Livezey, 1987).

We consider interannual SSH variations in (a) the North Atlantic (i.e. the work of §3.1) and (b) the Azores Subtropical Front (§3.2.1 above). As a measure of the strength of a mode of SSH variability, we use the amplitude of the corresponding principal component. For both case (a) and (b) we calculated the cross-correlation coefficient ( $r$ ) between the climate index (NAO and EAP) and the strength of each of the two leading complex EOFs. Table 4 summarises the results. We see that the NAO is correlated

## SSH Variability in the North Atlantic

D. Cromwell

[Title Page](#)

[Abstract](#)

[Introduction](#)

[Conclusions](#)

[References](#)

[Tables](#)

[Figures](#)

[◀](#)

[▶](#)

[◀](#)

[▶](#)

[Back](#)

[Close](#)

[Full Screen / Esc](#)

[Printer-friendly Version](#)

[Interactive Discussion](#)

only very weakly, if at all, with the leading principal component amplitudes of SSH variability. Indeed, in the Azores Subtropical Region, there is a hint of a very weak anti-correlation between the NAO and the amplitude of PC2. This is not altogether surprising: we noted earlier that although the spatial pattern of the leading mode has a tripole structure it is different from the SST tripole associated with the NAO. Temporal variability of the NAO likely maps onto more than simply the leading mode of SSH variability.

In contrast, the EAP is correlated with the two leading modes of SSH variability, particularly with PC2 in the Azores Subtropical Front region, where  $r=0.22$ . The cross-correlations of the two leading modes of SSH variability with the EAP index exceed the 95% confidence level. The small values of  $r$  indicate that, although this mode of atmospheric pressure variability plays a significant role in explaining these modes of SSH variance, it is not the dominating factor. Modelling studies, beyond the scope of this study, would be required to investigate the relative role of possible forcing mechanisms such as baroclinic instability, bursts in wind stress or seasonal variations in local currents.

#### 4 Discussion and conclusions

We have investigated the variability of sea surface height in the North Atlantic basin using a merged DUACS altimeter dataset spanning October 1992–January 2004. By applying complex empirical orthogonal function analysis we determined the spatial and temporal structure of SSH variability, including evidence of propagating features, for the leading four modes. Using wavelet analysis we determined the time-varying spectral density content of the principal components. We began by investigating the interannual variability in the North Atlantic by lowpass filtering the SSH data at a cutoff of 18 months. The spatial pattern of the leading complex EOF, comprising 30% of the total variability, showed a tripole structure with a connecting ridge between the high-latitude region and the subtropics along the eastern boundary. The regions of strong variability

#### SSH Variability in the North Atlantic

D. Cromwell

[Title Page](#)

[Abstract](#)

[Introduction](#)

[Conclusions](#)

[References](#)

[Tables](#)

[Figures](#)

[◀](#)

[▶](#)

[◀](#)

[▶](#)

[Back](#)

[Close](#)

[Full Screen / Esc](#)

[Printer-friendly Version](#)

[Interactive Discussion](#)

EGU

in the subtropics and subpolar gyre are linked by a 5-year signal propagating north along the eastern boundary. Rotation of CEOF phase arrows also indicates SSH propagation at 5-year periodicity in the Labrador Sea. The second mode, with a strong 3-year phase signal, is concentrated in the eastern subtropical gyre and may be linked to the low-frequency East Atlantic Pattern of atmospheric pressure variability.

We also focussed on the Azores subtropical front region of the northeast Atlantic. The leading mode (35% of the total variability) is strong in the south and east of this region. A dominant 3-year signal suggests that the EAP may be playing an important role in forcing SSH variability in this dynamic region. The second mode (21%) has a near-zonal band of lower variance between  $\sim 22^{\circ}$ – $27^{\circ}$  N sandwiched between two regions of higher variance.

In order to retain SSH signatures associated with propagating baroclinic Rossby waves we also lowpass filtered the altimeter data in the northeast Atlantic at a 30-day (rather than 18-month) cutoff. The strongest mode is the annual steric signal, representing 46% of the SSH variability. The second mode, with dominant timescales at  $\sim 3$  years,  $\sim 1$  year and 6 months accounts for 10% of the remaining variability. The third and fourth CEOFs, together accounting for 11% of the non-steric variability, are associated with westward propagating subannual Rossby waves which are particularly marked in a “waveband” between  $\sim 32^{\circ}$ – $36^{\circ}$  N. We showed the detailed trajectory of the westward propagating energy in this waveband. Peaks in the strength of this signal are observed in the region in 1996, 1997, 1999 and 2003, presumably linked to strong forcing then.

No significant cross-correlation is found between the North Atlantic Oscillation and the amplitude of the leading two principal components of interannual SSH variability for either the North Atlantic basin or the subregion around the Azores subtropical front. The East Atlantic Pattern, by contrast, is correlated with the principal components of the two leading modes of SSH variability, particularly with PC2 in the Azores subtropical frontal region.

We intend to extend the work presented here by analysing other datasets including

---

## SSH Variability in the North Atlantic

D. Cromwell

---

[Title Page](#)

[Abstract](#)

[Introduction](#)

[Conclusions](#)

[References](#)

[Tables](#)

[Figures](#)

◀

▶

◀

▶

[Back](#)

[Close](#)

[Full Screen / Esc](#)

[Printer-friendly Version](#)

[Interactive Discussion](#)

sea surface temperature and chlorophyll to shed further light on the variability and dynamics of the North Atlantic Ocean. Killworth et al. (2004), for example, have shown the potential for discriminating between different mechanisms involved in baroclinic Rossby wave propagation by combining sea surface height and chlorophyll observations from space. Further work on plausible forcing mechanisms on SSH variability could be investigated by comparing hindcasts for the observed time period of 1992–2004 from an ocean general circulation model with satellite and hydrographic measurements. Modelling studies, such as Eden and Willebrand (2001), have shown how hindcasts can shed light on mechanisms of interannual to decadal variability in North Atlantic SSH signatures and circulation. Bellucci and Richards (2006) also show the fruitfulness of such an approach in their model investigation of the effect of decadal NAO variability on the ocean circulation in the North Atlantic. A combination of similar modelling and observational approaches will improve our ability to detect changes in the meridional overturning circulation which is of such importance to the climate system.

15 **Acknowledgements.** DUACS altimeter data were produced and kindly provided by the CLS Space Oceanography Division. Paolo Cipollini helped make these data available to colleagues within the Laboratory for Satellite Oceanography at NOCS. Wavelet software was provided by Christopher Torrence and Gilbert Compo, and is available at: <http://paos.colorado.edu/research/wavelets>. The author gratefully acknowledges useful discussions with several colleagues, especially P. Challenor, J. Harle, A. Hogg, J. Hirschi, S. Josey and B. Topliss. This work was funded under the Ocean Variability and Climate core strategic programme of the UK's Natural Environment Research Council.

## References

25 Barnston, A. G. and R. E. Livezey: Classification, seasonality and persistence of low-frequency atmospheric circulation patterns, *Mon. Weather Rev.*, 115, 1083–1126, 1987.

Bellucci, A. and Richards, K. J.: Effects of NAO variability on the North Atlantic Ocean circulation, *Geophys. Res. Lett.*, 33, L02612, doi:10.1029/2005GL024890, 2006.

Broecker, W. S.: The great ocean conveyor, *Oceanography*, 4, 79–89, 1991.

[Title Page](#)[Abstract](#)[Introduction](#)[Conclusions](#)[References](#)[Tables](#)[Figures](#)[|◀](#)[▶|](#)[◀](#)[▶](#)[Back](#)[Close](#)[Full Screen / Esc](#)[Printer-friendly Version](#)[Interactive Discussion](#)

## SSH Variability in the North Atlantic

D. Cromwell

[Title Page](#)[Abstract](#)[Introduction](#)[Conclusions](#)[References](#)[Tables](#)[Figures](#)[◀](#)[▶](#)[◀](#)[▶](#)[Back](#)[Close](#)[Full Screen / Esc](#)[Printer-friendly Version](#)[Interactive Discussion](#)

EGU

Bryden, H. L., Longworth, H. R., and Cunningham, S. A.: Slowing of the Atlantic meridional overturning circulation at 25° N, *Nature*, 438, 655–657, 2005.

Chelton, D. B. and Schlax, M. G.: Global observations of oceanic Rossby waves, *Science*, 272, 234–238, 1996.

5 Cipollini, P., Cromwell, D., Jones, M. S., Quartly, G. D., and Challenor, P. G.: Concurrent altimeter and infrared observations of Rossby wave propagation near 34° N in the Northeast Atlantic, *Geophysical Research Letters*, 24, 889–892, 1997.

10 Cipollini, P., Cromwell, D., and Quartly, G. D.: Observations of Rossby wave propagation in the northeast Atlantic with TOPEX/POSEIDON altimetry, *Advances in Space Research* 22, 1553–1556, 1998.

CLS: SSALTO/DUACS user handbook : (M)SLA and (M)ADT near-real time and delayed time products, Ramonville St-Agne-FRANCE CLS-DOS-NT-04.103, 2004.

Cromwell, D.: Sea surface height observations of the 34° N “waveguide” in the North Atlantic, *Geophys. Res. Lett.*, 28, 3705–3708, 2001.

15 Eden, C. and Willebrand, J.: Mechanism of Interannual to Decadal Variability of the North Atlantic Circulation, *J. Clim.*, 14, 2266–2280, 2001.

Farge, M.: Wavelet transforms and their applications to turbulence, *Annual Review of Fluid Mechanics*, 24, 395–457, 1992.

Foufoula-Georgiou, E. and Kumar, P.: *Wavelets in Geophysics*, San Diego, Academic Press, 20 1994.

Fu, L.-L.: The interannual variability of the North Atlantic Ocean revealed by combined data from TOPEX/Poseidon and Jason altimetric measurements, *Geophys Res. Lett.*, 31, L23303, doi:10.1029/2004GL021200, 2004.

Gill, A. E.: *Atmosphere-Ocean Dynamics*, San Diego, Academic Press, 662, 1982.

25 Häkkinen, S.: Variability in sea surface height: A qualitative measure for the meridional overturning in the North Atlantic, *J. Geophys. Res.*, 106, 13 837–13 848, 2001.

Häkkinen, S. and Rhines, P. B.: Decline of Subpolar North Atlantic Circulation During the 1990s, *Science*, 304, 555–559, 2004.

Jacobs, G. A., Hurlburt, H. E., Kindle, J. C., Metzger, E. J., Mitchell, J. L., Teague, W. J., and 30 Wallcraft, A. J.: Decade-scale trans-Pacific propagation and warming effects of an El Niño anomaly, *Nature*, 370, 360–363, 1994.

Killworth, P. D., Cipollini, P., Uz, B. M., and Blundell, J. R.: Physical and biological mechanisms for planetary waves observed in sea-surface chlorophyll, *J. Geophys. Res.*, 109, C07002,

doi:10.1029/2003JC001768, 2004.

Le Traon, P. Y., and Ogor, F.: ERS-1/2 orbit improvement using TOPEX/Poseidon: the 2 cm challenge, *J. Geophys. Res.*, 103, 8045–8057, 1998.

Le Traon, P. Y., Nadal, F., and Ducet, N.: An improved mapping method of multi-satellite altimeter data, *J. Atmos. Oceanic Technol.*, 25, 522–534, 1998.

Levermann, A., Griesel, A., Hofmann, M., Montoya, M., and Rahmstorf, S.: Dynamic sea level changes following changes in the thermohaline circulation, *Clim. Dyn.*, 24, 347–354, 2005.

Pingree, R. D.: The eastern Subtropical gyre (North Atlantic): Flow Rings Recirculations Structure and Subduction, *J. Marine Biological Association of the United Kingdom*, 77, 573–624, 1997.

Pingree, R. D.: Ocean structure and climate (Eastern North Atlantic): in situ measurement and remote sensing (altimeter), *Journal of the Marine Biological Association of the UK*, 82, 681–707, 2002.

Schiermeier, Q.: A sea change, *Nature*, 439, 256–260, 2006.

Tokmakian, R. T. and Challenor, P. G.: Observations in the Canary Basin and the Azores Frontal Region Using Geosat Data, *J. Geophys. Res.* 98, 4761–4773, 1993.

Torrence, C. and Compo, G. P.: practical guide to wavelet analysis, *Bulletin of the American Meteorological Society*, 79, 61–78, 1998.

Tourre, Y. M., Kushnir, Y., and White, W. B.: Evolution of Interdecadal Variability in Sea Level Pressure, Sea Surface Temperature, and Upper Ocean Temperature over the Pacific Ocean, *Journal of Physical Oceanography*, 29, 1528–1541, 1999.

Tychensky, A., Le Traon, P. Y., Hernandez, F., and Jourdan, D.: Large structures and temporal change in the Azores Front during the SEMAPHORE experiment, *J. Geophys. Res.*, 103, 25 009–25 027, 1998.

von Storch, H. and Zwiers, F. W.: *Statistical Analysis in Climate Research*, Cambridge University Press, 1999.

OSD

3, 609–636, 2006

---

## SSH Variability in the North Atlantic

D. Cromwell

---

[Title Page](#)

[Abstract](#)

[Introduction](#)

[Conclusions](#)

[References](#)

[Tables](#)

[Figures](#)

◀

▶

◀

▶

[Back](#)

[Close](#)

[Full Screen / Esc](#)

[Printer-friendly Version](#)

[Interactive Discussion](#)

EGU

## SSH Variability in the North Atlantic

D. Cromwell

**Table 1.** Summary of the characteristics of the leading four complex EOF modes of DUACS altimeter sea surface height anomaly measurements in the North Atlantic basin ( $10^{\circ}$ – $65^{\circ}$  N,  $80^{\circ}$ – $0^{\circ}$  W) for the period October 1992–January 2004. The input data are on a regular  $1^{\circ} \times 1^{\circ}$  grid, have a sampling period of 1 week and have been lowpass filtered to remove periods shorter than 18 months.

Mode	% Variability	Dominant timescales	Notable features
1	30	~5 years	Tripole structure; connecting ridge of high variability at eastern boundary.
2	17	~3 years	High variability in eastern subtropical gyre and in western tropics. Amplitude low in 1997.
3	15	~2 years, ~4 years	High variability in western tropics, Gulf Stream extension, Labrador Sea and in region of mid-Atlantic Ridge north of $\sim 35^{\circ}$ N.
4	12	> 3 years	Isolated patches as well as ridges of high variability, notably in western Labrador Sea. Amplitude peak in 2001.

[Title Page](#)[Abstract](#)[Introduction](#)[Conclusions](#)[References](#)[Tables](#)[Figures](#)[|◀](#)[▶|](#)[◀](#)[▶](#)[Back](#)[Close](#)[Full Screen / Esc](#)[Printer-friendly Version](#)[Interactive Discussion](#)

EGU

## SSH Variability in the North Atlantic

D. Cromwell

**Table 2.** Summary of the characteristics of the leading four complex EOF modes of DUACS altimeter sea surface height anomaly measurements in the northeast Atlantic ( $20^{\circ}$ – $40^{\circ}$  N,  $50^{\circ}$ – $10^{\circ}$  W) for the period October 1992–January 2004. The input data are on a high-resolution Mercator grid of  $(1/3)^{\circ}$  in longitude  $\times (1/3)^{\circ} \cos(\text{latitude})$  in latitude, have a sampling period of 1 week and have been lowpass filtered to remove periods shorter than 18 months.

Mode	% Variability	Dominant timescales	Notable features
1	35	~3 years, ~5 years	Strong variability south of $30^{\circ}$ N and also everywhere east of $\sim 25^{\circ}$ W; one order of magnitude lower variability elsewhere.
2	21	~2 years, ~5 years	Near-zonal band of low variance at $\sim 22^{\circ}$ – $27^{\circ}$ N sandwiched between two regions of higher variance. Again, the levels of variance span around one order of magnitude. Phase propagation with period of 2 years peaks in 2001.
3	13	~3 years	Ridges and local patches of high variability, including near-zonal band at $28^{\circ}$ N. Peak in phase propagation in 1997.
4	10	~4 years	A few local patches of moderate variability, mostly west of $35^{\circ}$ W. Strongest phase propagation between 1998–2001.

[Title Page](#)[Abstract](#)[Introduction](#)[Conclusions](#)[References](#)[Tables](#)[Figures](#)[|◀](#)[▶|](#)[◀](#)[▶](#)[Back](#)[Close](#)[Full Screen / Esc](#)[Printer-friendly Version](#)[Interactive Discussion](#)

EGU

**Table 3.** Summary of the characteristics of the leading four complex EOF modes of DUACS altimeter sea surface height anomaly measurements in the Azores Subtropical Front region ( $20^{\circ}$ – $40^{\circ}$  N,  $50^{\circ}$ – $10^{\circ}$  W) for the period October 1992–January 2004. The input data are on a high-resolution Mercator grid of  $(1/3)^{\circ}$  in longitude  $\times (1/3)^{\circ} \cos(\text{latitude})$  in latitude, have a sampling period of 1 week and have been lowpass filtered to remove periods shorter than 30 days.

Mode	% Variability	Dominant timescales	Notable features
1	46	Annual	Steric cycle
2	5	$\sim 3$ years $\sim 1$ year $\sim 6$ months	Peak in 1996 Observed between 2000–2002 Phase propagation observed 2001–2003
3	2.9	$\sim 6$ – $10$ months	Westward propagating baroclinic Rossby waves and/or eddies. concentration of SSH variability in a near zonal band around $32^{\circ}$ – $36^{\circ}$ N. Energy peaks occur in winters of 1996, 1997, 1999 and 2003.
4	2.8	$\sim 6$ – $10$ months	Similar characteristics to CEOF 3

## SSH Variability in the North Atlantic

D. Cromwell

[Title Page](#)

[Abstract](#)

[Introduction](#)

[Conclusions](#)

[References](#)

[Tables](#)

[Figures](#)

[◀](#)

[▶](#)

[◀](#)

[▶](#)

[Back](#)

[Close](#)

[Full Screen / Esc](#)

[Printer-friendly Version](#)

[Interactive Discussion](#)

EGU

## SSH Variability in the North Atlantic

D. Cromwell

**Table 4.** Cross-correlation coefficient ( $r$ ) between climate indices NAO (North Atlantic Oscillation), EAP (East Atlantic Pattern) and the principal component amplitudes of the two leading complex EOFs in the North Atlantic (10°–65° N, 80°–0° W) and Azores Subtropical Front (20°–40° N, 50°–10° W) regions. Values of  $r$  in **bold** are statistically significant at the 95% confidence level.

		NAO	EAP
North Atlantic	PC1	0.009	<b>0.19</b>
	PC2	0.012	<b>0.17</b>
Subtropical Front	PC1	0.07	<b>0.18</b>
	PC2	−0.09	<b>0.22</b>

[Title Page](#)[Abstract](#)[Introduction](#)[Conclusions](#)[References](#)[Tables](#)[Figures](#)[|◀](#)[▶|](#)[◀](#)[▶](#)[Back](#)[Close](#)[Full Screen / Esc](#)[Printer-friendly Version](#)[Interactive Discussion](#)

EGU

## SSH Variability in the North Atlantic

D. Cromwell

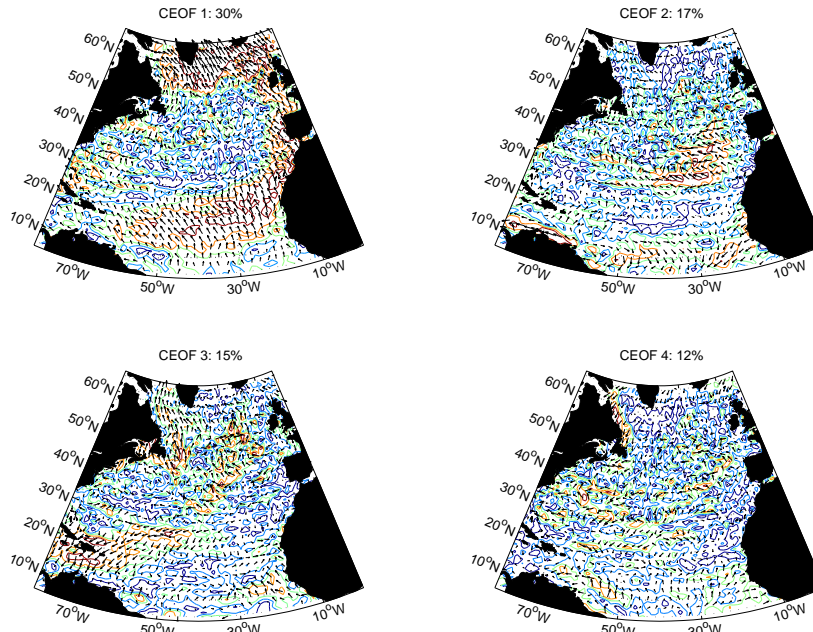


**Fig. 1.** Results of a complex empirical orthogonal function (CEOF) analysis of DUACS altimeter sea surface height anomaly measurements in the North Atlantic basin ( $10^{\circ}$ – $65^{\circ}$  N,  $80^{\circ}$ – $0^{\circ}$  W) for the period October 1992–January 2004. The input data are on a regular  $1^{\circ} \times 1^{\circ}$  grid, have a sampling period of 1 week and have been lowpass filtered to remove periods shorter than 18 months. Maps of first four CEOF modes with amplitude contours (in arbitrary units) and phase overlaid as arrows (anticlockwise rotation of phase arrows from one location of strong amplitude to another indicates propagating signal). The title of each subplot gives the mode number and its percentage contribution to the total variability.

[Title Page](#)[Abstract](#)[Introduction](#)[Conclusions](#)[References](#)[Tables](#)[Figures](#)[|◀](#)[▶|](#)[◀](#)[▶](#)[Back](#)[Close](#)[Full Screen / Esc](#)[Printer-friendly Version](#)[Interactive Discussion](#)

## SSH Variability in the North Atlantic

D. Cromwell

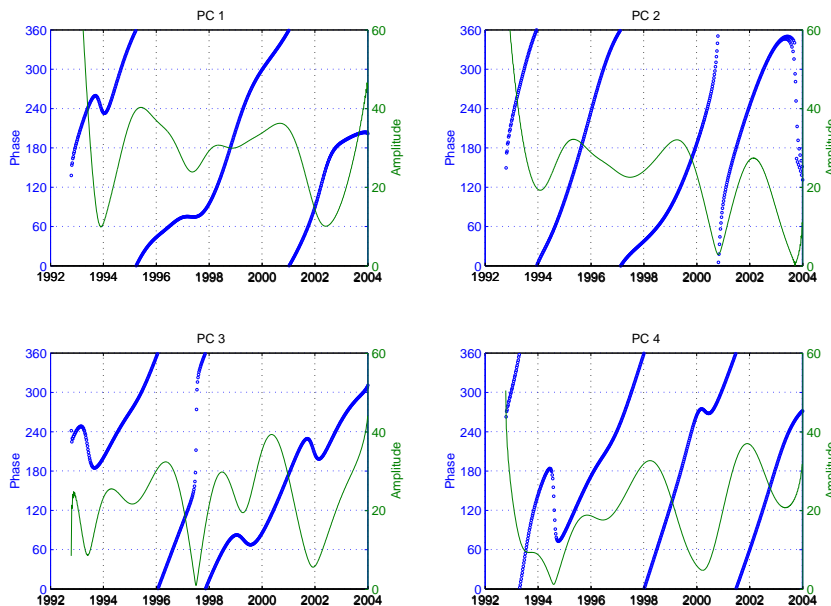


**Fig. 2.** Principal component time series corresponding to the maps of CEOF modes plotted in Fig. 1 (North Atlantic SSH anomalies,  $1^\circ \times 1^\circ$  gridding, lowpass filtered at 18 months). Both phase (in degrees; blue) and amplitude (arbitrary units; green) are shown.

[Title Page](#)

[Abstract](#) [Introduction](#)

[Conclusions](#) [References](#)

[Tables](#) [Figures](#)

[◀](#) [▶](#)

[◀](#) [▶](#)

[Back](#) [Close](#)

[Full Screen / Esc](#)

[Printer-friendly Version](#)

[Interactive Discussion](#)

## SSH Variability in the North Atlantic

D. Cromwell

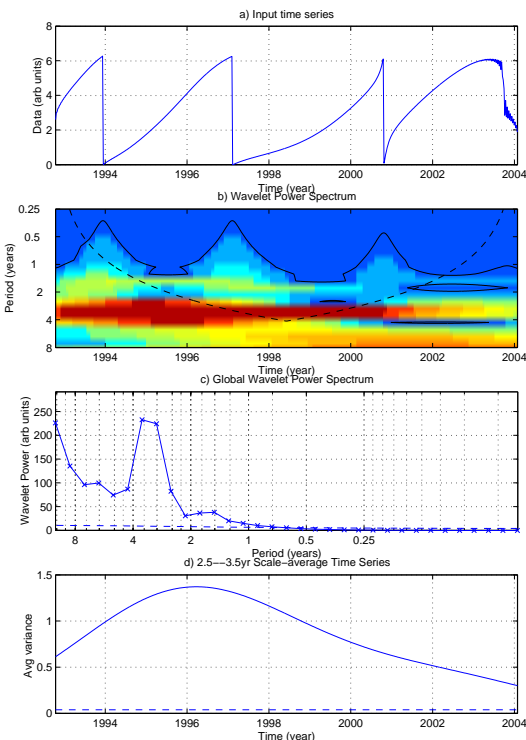


**Fig. 3.** Wavelet analysis of the principal component phase associated with the second CEOF in sea surface height anomaly in the North Atlantic (PC2 in Fig. 2). **(a)** Input time series, i.e. the phase of PC2; **(b)** wavelet power spectrum of (a); **(c)** global wavelet power spectrum, i.e. integral of (b) over time; **(d)** time series of scale average of (b) in period range 2.5–3.5 years. In (b), the dashed line indicates the cone of influence, below which edge effects become important, and the solid contour is the 95% confidence level. In (c) and (d), the 95% confidence level is indicated by a dashed line.

[Title Page](#)[Abstract](#)[Introduction](#)[Conclusions](#)[References](#)[Tables](#)[Figures](#)[◀](#)[▶](#)[◀](#)[▶](#)[Back](#)[Close](#)[Full Screen / Esc](#)[Printer-friendly Version](#)[Interactive Discussion](#)

## SSH Variability in the North Atlantic

D. Cromwell

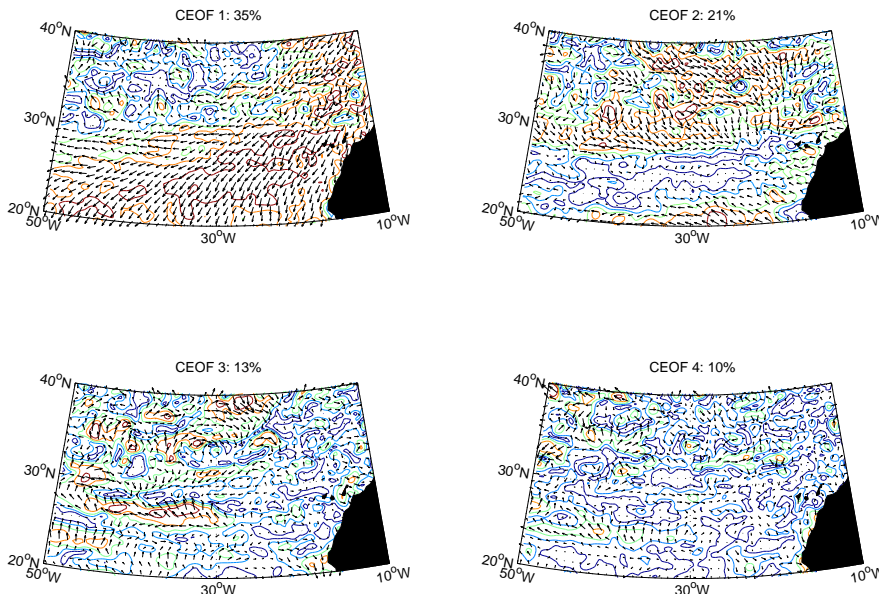


**Fig. 4.** Results of a complex empirical orthogonal function (CEOFO) analysis of DUACS altimeter sea surface height anomaly measurements in the northeast Atlantic basin ( $20^{\circ}$ – $40^{\circ}$  N,  $50^{\circ}$ – $10^{\circ}$  W) for the period October 1992–January 2004. The input data are on a Mercator ( $1/3^{\circ}$  longitude  $\times$  ( $1/3^{\circ}$ )  $\cos(\text{latitude})$ ) latitude grid, have a sampling period of 1 week and have been lowpass filtered to remove periods shorter than 18 months. Maps of first four CEOFO modes with amplitude contours (in arbitrary units) and phase overlaid as arrows (anticlockwise rotation of phase arrows from one location of strong amplitude to another indicates propagating signal). The title of each subplot gives the mode number and its percentage contribution to the total variability.

[Title Page](#)[Abstract](#)[Introduction](#)[Conclusions](#)[References](#)[Tables](#)[Figures](#)[|◀](#)[▶|](#)[◀](#)[▶](#)[Back](#)[Close](#)[Full Screen / Esc](#)[Printer-friendly Version](#)[Interactive Discussion](#)

## SSH Variability in the North Atlantic

D. Cromwell

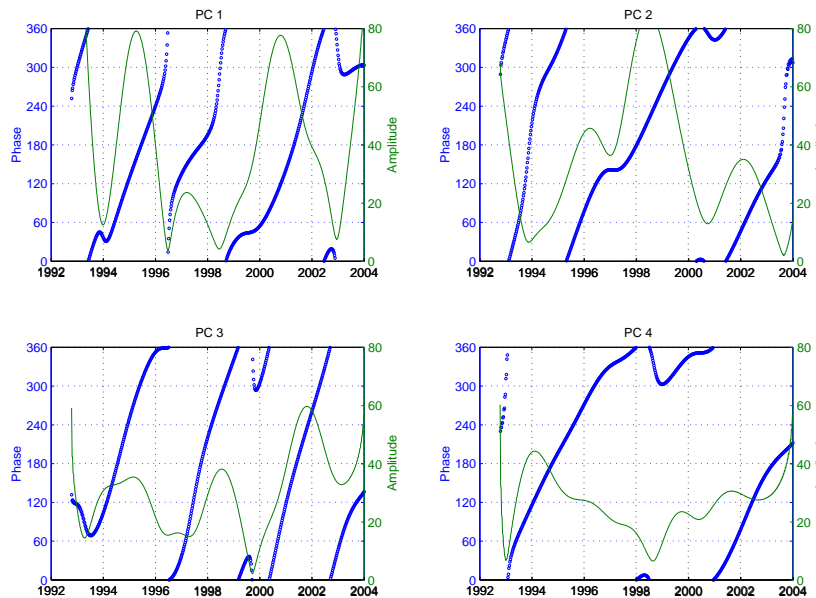


**Fig. 5.** Principal component time series corresponding to the maps of CEOF modes plotted in Fig. 4 (northeast Atlantic SSH anomalies,  $(1/3)^\circ \times (1/3)^\circ \cos(\text{latitude})$  grid, lowpass filtered at 18 months). Both phase (in degrees; blue) and amplitude (arbitrary units; green) are shown.

<a href="#">Title Page</a>	
<a href="#">Abstract</a>	<a href="#">Introduction</a>
<a href="#">Conclusions</a>	<a href="#">References</a>
<a href="#">Tables</a>	<a href="#">Figures</a>
<a href="#">◀</a>	<a href="#">▶</a>
<a href="#">◀</a>	<a href="#">▶</a>
<a href="#">Back</a>	<a href="#">Close</a>
<a href="#">Full Screen / Esc</a>	
<a href="#">Printer-friendly Version</a>	
<a href="#">Interactive Discussion</a>	

## SSH Variability in the North Atlantic

D. Cromwell

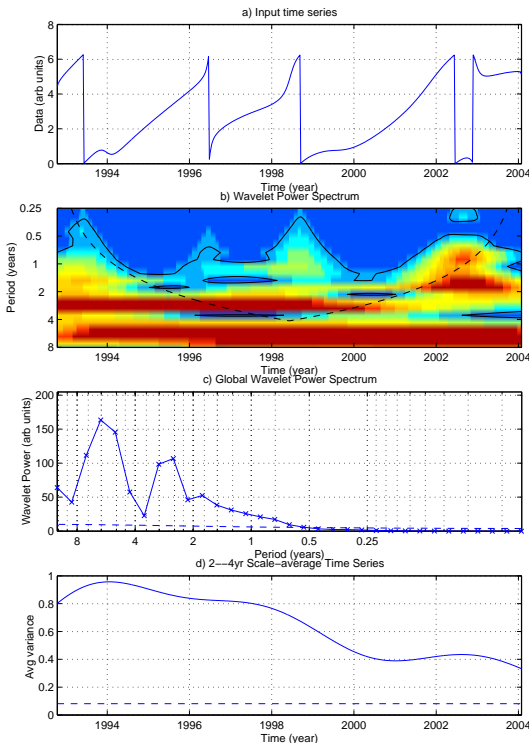


**Fig. 6.** Wavelet analysis of the principal component phase associated with the leading CEOF in sea surface height anomaly over the northeast Atlantic (PC1 of Fig. 5). The dataset has been lowpass filtered to remove signals shorter than 18 months. **(a)** Input time series, i.e. the phase of PC1; **(b)** wavelet power spectrum of (a); **(c)** global wavelet power spectrum, i.e. integral of (b) over time; **(d)** time series of scale average of (b) for periods in range 2–4 years. In (b), the dashed line indicates the cone of influence, below which edge effects become important, and the solid contour is the 95% confidence level. In (c) and (d), the 95% confidence level is indicated by a dashed line.

[Title Page](#)[Abstract](#)[Introduction](#)[Conclusions](#)[References](#)[Tables](#)[Figures](#)[|◀](#)[▶|](#)[◀](#)[▶](#)[Back](#)[Close](#)[Full Screen / Esc](#)[Printer-friendly Version](#)[Interactive Discussion](#)

## SSH Variability in the North Atlantic

D. Cromwell

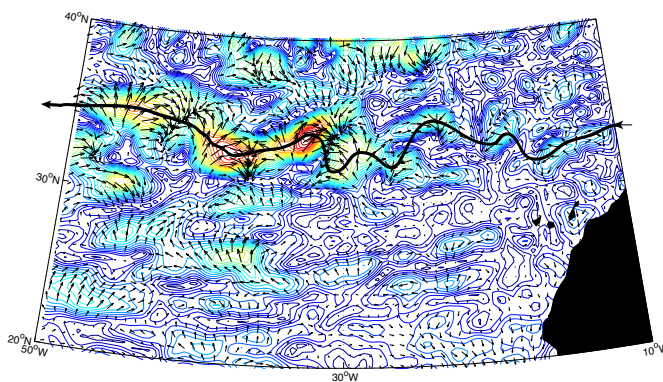


**Fig. 7.** Spatial pattern of 3rd CEOF of sea surface height anomaly in northeast Atlantic after lowpass filtering at 30 days. Both amplitude (coloured contours; arbitrary units) and phase (arrows) are shown. Phase rotation in the zonal band  $\sim 32^{\circ}$ – $36^{\circ}$  N west of  $\sim 30^{\circ}$  W is characteristic of the westward propagation of baroclinic Rossby waves in this region. The solid black line indicates the observed trajectory of the Rossby waves.

[Title Page](#)[Abstract](#)[Introduction](#)[Conclusions](#)[References](#)[Tables](#)[Figures](#)[|◀](#)[▶|](#)[◀](#)[▶](#)[Back](#)[Close](#)[Full Screen / Esc](#)[Printer-friendly Version](#)[Interactive Discussion](#)

EGU

## SSH Variability in the North Atlantic

D. Cromwell

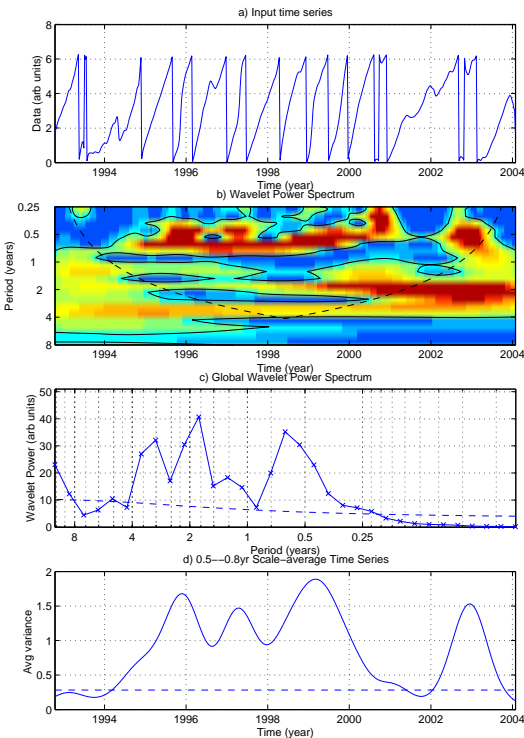


**Fig. 8.** Wavelet analysis of the principal component phase associated with the 3rd CEOF in sea surface height over the northeast Atlantic. The dataset has been lowpass filtered to remove signals shorter than 30 days, thus retaining subannual variability. **(a)** Input time series, i.e. the phase of the 3rd principal component; **(b)** wavelet power spectrum of (a); **(c)** global wavelet power spectrum, i.e. integral of (b) over time; **(d)** time series of scale average of (b) for periods in range 0.5–0.8 years (~6–10 months), corresponding to baroclinic Rossby waves at this latitude. In (b), the dashed line indicates the cone of influence, below which edge effects become important, and the solid contour is the 95% confidence level. In (c) and (d), the 95% confidence level is indicated by a dashed line.

[Title Page](#)[Abstract](#)[Introduction](#)[Conclusions](#)[References](#)[Tables](#)[Figures](#)[|◀](#)[▶|](#)[◀](#)[▶](#)[Back](#)[Close](#)[Full Screen / Esc](#)[Printer-friendly Version](#)[Interactive Discussion](#)